

Viscous flow in a soft valve

K. Park¹, A. Tixier², A. H. Christensen¹, S. F. Arnbjerg-Nielsen,
M. A. Zwieniecki² and K. H. Jensen¹†

¹Department of Physics, Technical University of Denmark, DK-2800 Kgs. Lyngby, Denmark

²Department of Plant Sciences, University of California, Davis, CA 95616, USA

(Received xx; revised xx; accepted xx)

Fluid-structure interactions are ubiquitous in nature and technology. However, the systems are often so complex that numerical simulations or ad hoc assumptions must be used to gain insight into the details of the complex interactions between the fluid and solid mechanics. In this paper, we present experiments and theory on viscous flow in a simple bioinspired soft valve which illustrate essential features of interactions between hydrodynamic and elastic forces at low Reynolds numbers. The setup comprises a sphere connected to a spring located inside a tapering cylindrical channel. The spring is aligned with the central axis of the channel and a pressure drop is applied across the sphere, thus forcing the liquid through the narrow gap between the sphere and the channel walls. The sphere's equilibrium position is determined by a balance between spring and hydrodynamic forces. Since the gap thickness changes with the sphere's position, the system has a pressure-dependent hydraulic resistance. This leads to a non-linear relation between applied pressure and flow rate: flow initially increases with pressure, but decreases when the pressure exceeds a certain critical value as the gap closes. To rationalize these observations, we propose a mathematical model that reduced the complexity of the flow to a two-dimensional lubrication approximation. A closed-form expression for the pressure-drop/flow rate is obtained which reveals that the flow rate Q depends on the pressure drop Δp , sphere radius a , gap thickness h_0 , and viscosity η as $Q \sim \eta^{-1} a^{1/2} h_0^{5/2} (\Delta p_c - \Delta p)^{5/2} \Delta p$, where the critical pressure Δp_c scales with the spring constant k and sphere radius a as $\Delta p_c \sim ka^{-2}$. These predictions compared favorably to the results of our experiments with no free parameters.

Key words: fluid-structure interactions, lubrication theory, low-Reynolds-number flow valve, biofluidynamics

1. Introduction

Fluid flow in flexible geometries occurs in many biological, medical, and industrial environments (Duprat & Stone 2015). Systems that couple the elasticity of a solid body with the motion of a fluid often have interesting properties; for instance, interactions between fluid-mechanical and elastic forces can lead to nonlinear pressure-drop/flow-rate relations (Grotberg & Jensen 2004; Heil & Hazel 2015) and the generation of instabilities (Heil & Hazel 2011), even in relatively simple channel geometries.

Soft channels and valves play important roles in biological fluid systems: from flexible veins that carry nutrients in animals (Heil & Hazel 2011) to valves which maintain

† Email address for correspondence: khjensen@fysik.dtu.dk, mzwienie@ucdavis.edu

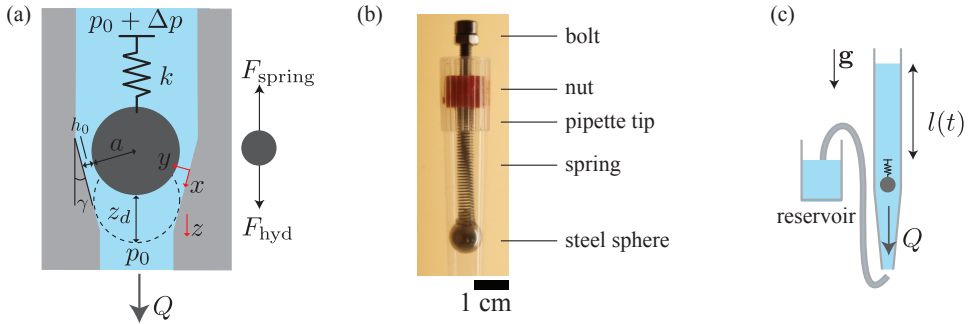


FIGURE 1. Schematics of the soft valve system and the experimental setup. (a) Schematic of the spring-actuated soft valve. A sphere of radius a is suspended from a spring (spring constant k) inside a tapering channel. The sphere’s position is determined by force equilibrium between hydrodynamic and force and spring forces. (b) Photograph of the setup showing the steel sphere, extension spring and pipette tip. (c) Schematic of the pressure-drop/flow-rate measurement system. The pressure-drop is controlled by the liquid column height $l(t)$, and the flow rate $Q = \pi(D/2)^2 dl/dt$ and pressure drop $\Delta p = \rho gl(t)$ is determined by image analysis (see additional details in text).

unidirectional flow through the human heart (Sotiropoulos *et al.* 2016). Soft valves are also relevant to fluid transport in plants, for instance, in torus-margo pit pores, microscopic channels that permit water flow between neighboring xylem tracheid conduits in plants (Choat *et al.* 2008; Jensen *et al.* 2016). The pore structure prevents air embolisms from spreading inside the plant by blocking the pore with a circular disc if a large pressure difference develops between adjacent tracheids. The disc is held in place by soft cellulose fibers which can deform elastically. This soft geometry may modify flow even in the absence of air embolisms, however, previous studies have assumed either a static geometry (Lancashire & Ennos 2002; Schulte 2012) or inviscid flows (Chapman *et al.* 1977), and the effect of fluid-structure interactions at low Reynolds numbers on this system is not currently well understood.

Systems that couple the elasticity of a solid body with the motion of a fluid link two sets of dynamics that, even when treated separately, can be quite complicated. The properties of biological channels and valves have been studied extensively, however, the geometry is often so complex that numerical simulations or ad hoc assumptions must be used to gain insight into the details of the complex interactions between the fluid and solid mechanics (Bellhouse & Talbot 1969; McCulloh *et al.* 2003; Kim & Bush 2012; Park *et al.* 2014; Yang *et al.* 2014; Gart *et al.* 2015; Jensen *et al.* 2016). Studies on models systems inspired by nature provide a promising alternative to *in-vivo* experiments or full-scale numerical simulations. For instance, experiments on microfluidic devices have demonstrated that fluid-induced deformation of elastic sheets and fibres in channels can influence the flow at low Reynolds numbers (Wexler *et al.* 2013; Ledesma-Alonso *et al.* 2014), and similar results have been obtained using external mechanical actuation (Holmes *et al.* 2013).

In this paper, we present experiments and theory on a simple spring-actuated valve system inspired by biology. It captures many of the non-linear interactions that characterizes flow in soft geometries where the hydraulic resistance varies with applied pressure. The valve is suitable for regulation of small-scale fluid flows and relevant to several biofluiddynamic problems. Moreover, the simple geometry allows us to derive a closed form solution, based on lubrication theory, which is compared to experimental data.

2. Experiment

We consider the effect of couplings between flow and elasticity on the idealized soft valve shown in Fig. 1(a): a sphere connected to an extension spring located inside a tapering cylindrical pipe. The spring is aligned with the central axis of the channel and a pressure drop Δp is applied across the sphere. The sphere's equilibrium position is determined by a balance between elastic and hydrodynamic forces. This leads to a non-linear relation between applied pressure Δp and flow rate $Q = \Delta p/R(\Delta p)$, where $R(\Delta p)$ is the pressure-dependent hydraulic resistance.

2.1. Experimental methods

The valve was fabricated using a steel sphere of radius $a = 5$ mm (KVJ Aktieselskab, 45RB5) which was glued onto an extension spring (spring constant $k = 0.16$ N/mm, RS Components 821-273), see Fig. 1(b). The spring and sphere was anchored to a M4 bolt that allowed us to control the vertical position of the sphere along the central axis of a 3 mL pipette tip of opening angle $\gamma = 0.024$ rad (alpha laboratories, LW8930). Finally, both ends of the the pipette was connected to silicone tubing (inner diameter $D = 12$ mm).

We used the hydrostatic pressure difference provided by a vertical liquid column of height $l(t)$ in the silicone tubing to drive flow across the valve, thus sweeping a broad range of pressure drops Δp in each experiment (Fig. 1(c)). The liquid column height $l(t)$ was tracked over time using image analysis of photographs captured using a digital camera (Canon, EOS 5D MARK III, 35mm Sigma lens F1.4 DG HSM Art) as described in Appendix A. The pressure drop $\Delta p = \rho gl(t)$ and flow rate $Q = \pi(D/2)^2 dl/dt$ was subsequently determined, where ρ is the liquid density and g is the gravitational acceleration (Fig. 1(c)). In the experiments, we varied the initial ball position in the range $z_d \sim 2.5 - 4.5$ mm (corresponding to initial gap thicknesses of $h_0 = z_d \sin \gamma \sim 60 - 110 \mu\text{m}$), and the liquid viscosity from DI water (1 cSt) to Silicon oil (100 cSt).

2.2. Observations

Our experiments reveal that the flow rate increases linearly with pressure when the pressure drop is relatively small, because the position of the sphere is not influenced by the flow (Fig. 2). However, as pressure increases, hydrodynamic forces push the sphere towards the channel wall, thus reducing the gap size h_0 (Fig. 1(a)). This leads to an increase in the resistance to flow. After reaching a maximum in flow Q_{\max} , at the pressure Δp_{\max} , the flow rate starts to decrease with increasing pressure and slowly approaches $Q = 0$ at the critical pressure drop Δp_c . The absolute magnitude of the flow can be tuned by varying the initial ball position z_d (and hence thickness of the gap between the sphere and tapering channel walls) or by changing the viscosity η of the fluid. We observe that both the peak flow rate Q_{\max} and optimum pressure Δp_{\max} increases with z_d . By contrast, only the flow rate Q appears to be affected significantly by variations in η .

The focus of our paper is predicting the flow rate as a function of the system parameters. In most our experiments, the Reynolds number $Re = (\rho Q)/(2\pi\eta a)$, is less than $\sim 10^{-3}$, and hence viscous effects dominate the flow. We take advantage of this by using steady-state lubrication theory in the following analysis. However, we note that when the Reynolds number is increased to $\sim 10^3$ (corresponding to an initial vertical displacement of $z_d = 5$ mm), periodic disturbances in the flow rate and sphere position can be observed (see appendix A and supplementary movie. 2). The observed pattern have features that resemble self-excited oscillations (see e.g. Luo & Pedley (1996)), but we shall leave its detailed consideration for future investigations.

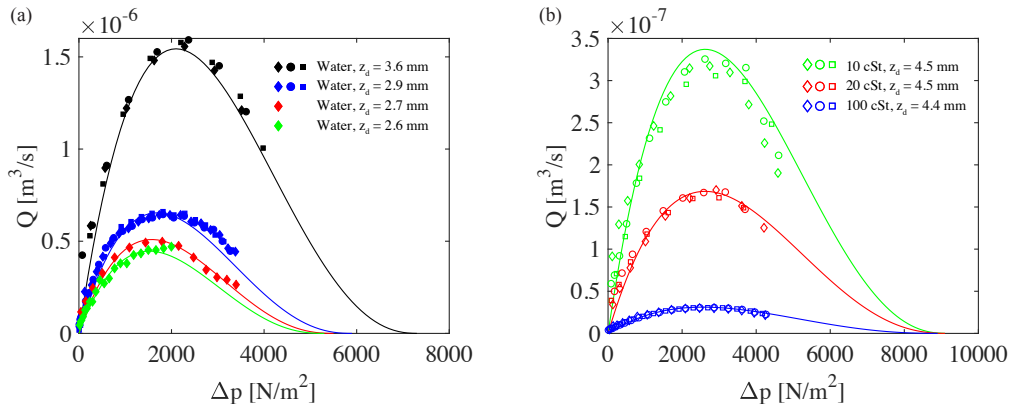


FIGURE 2. Pressure-drop/flow rate relation for viscous flow in a soft valve. (a) Flow rate Q plotted as a function of applied pressure Δp for DI water flow with viscosity $\eta = 1$ cSt, spring constant $k = 0.16$ N/mm, and sphere radius $a = 5$ mm. Results for initial ball position $z_d = 2.6, 2.7, 2.9$, and 3.6 mm are shown as green, red, blue and black symbols, respectively. (b) Flow rate Q plotted as a function of applied pressure Δp for silicone oil with initial ball position $z_d \sim 4.5$ mm, spring constant $k = 0.16$ N/mm, and sphere radius $a = 5$ mm. Results for viscosities $\eta = 10, 20$, and 100 cSt are shown as green, red, and blue symbols, respectively.

3. Theory

To rationalize the experimental observations (Fig. 2), we seek to characterize the pressure-drop/flow rate relation as a function of the system parameters

$$Q = \frac{\Delta p}{R}. \quad (3.1)$$

The pressure-dependent hydraulic resistance $R(\Delta p)$ is a function of the vertical position z of the sphere, which in turn is determined by the force-balance on the sphere due to spring- and hydrodynamics forces along the z -axis (Fig. 1(a)):

$$F_{\text{spring}} + F_{\text{hyd}} = 0. \quad (3.2)$$

We proceed in two steps to compute the pressure-dependent resistance R in Eq. (3.1): First, we use lubrication theory to determine the flow field in the narrow gap between the sphere and the tapering channel walls for a fixed vertical position of the sphere and pressure drop Δp . This leads to a position-dependent hydraulic resistance $R(z)$. Our analysis of the static problem follows Smistrup & Stone (2007), who considered a magnetically actuated ball valve. Then, we use the force-balance equation (3.2) to solve for the equilibrium position $z_{\text{eq}}(\Delta p)$ which leads to an expression for $R(\Delta p)$.

The valve system comprises a sphere connected to a spring in a tapering cylindrical channel with opening angle γ (Fig. 1(a)). In the experiments, the sphere radius is $a = 5 \times 10^{-3}$ m while the typical size of the gap between the sphere and the channel walls is $h_0 \leq 10^{-4}$ m. We therefore consider the limit where the gap is narrow ($h_0 \ll a$), and let βa denote the vertical displacement of the sphere above the point of contact where $h_0 = 0$ and $\beta = 0$. The gap thickness can then be expressed in terms of β and the sphere radius a , and opening angle γ as $h_0 = a\beta \sin(\gamma)$. Because the gap is narrow, the coordinate system can locally be considered as Cartesian, with x - and y -axes indicated in Fig. 1(a). Note that the z -axis in the diagram does not belong to this coordinate system.

3.1. Lubrication theory

The flow is governed by the Navier-Stokes and continuity equations

$$\rho \left[\frac{\partial \mathbf{u}}{\partial t} + (\mathbf{u} \cdot \nabla) \mathbf{u} \right] = -\nabla p + \eta \nabla^2 \mathbf{u} \quad (3.3)$$

$$\nabla \cdot \mathbf{u} = 0 \quad (3.4)$$

where ρ denotes the density, η the viscosity, p the pressure, and \mathbf{u} the velocity field. In the steady low-Reynolds-number limit, the Navier-Stokes and continuity equations for the flow in the gap reduces to

$$\eta \left(\frac{\partial^2 u_x}{\partial x^2} + \frac{\partial^2 u_x}{\partial y^2} \right) = \frac{\partial p}{\partial x} \quad (3.5a)$$

$$\eta \left(\frac{\partial^2 u_y}{\partial x^2} + \frac{\partial^2 u_y}{\partial y^2} \right) = \frac{\partial p}{\partial y} \quad (3.5b)$$

$$\frac{\partial u_x}{\partial x} + \frac{\partial u_y}{\partial y} = 0 \quad (3.5c)$$

We non-dimensionalize using the variables

$$X = \frac{x}{a}, \quad Y = \frac{y}{h_0}, \quad U_X = \frac{u_x}{q_0/h_0}, \quad U_Y = \frac{u_y}{q_0/a}, \quad P = \frac{p}{\eta q_0 a / h_0^3} \quad (3.6)$$

where q_0 is a constant flow rate per unit width. Equations (3.5a)-(3.5c) then become

$$\left(\frac{h_0}{a} \right)^2 \frac{\partial^2 U_X}{\partial X^2} + \frac{\partial^2 U_X}{\partial Y^2} = \frac{\partial P}{\partial X} \quad (3.7a)$$

$$\left(\frac{h_0}{a} \right)^4 \frac{\partial^2 U_Y}{\partial X^2} + \left(\frac{h_0}{a} \right)^2 \frac{\partial^2 U_Y}{\partial Y^2} = \frac{\partial P}{\partial Y} \quad (3.7b)$$

$$\frac{\partial U_X}{\partial X} + \frac{\partial U_Y}{\partial Y} = 0 \quad (3.7c)$$

Taking the narrow-gap-limit ($h_0/a \ll 1$), the dimensional lubrication equations are obtained

$$\eta \frac{\partial^2 u_x}{\partial y^2} = \frac{\partial p}{\partial x} \quad (3.8a)$$

$$0 = \frac{\partial p}{\partial y} \quad (3.8b)$$

$$\frac{\partial u_x}{\partial x} + \frac{\partial u_y}{\partial y} = 0 \quad (3.8c)$$

From equation (3.8b) it is seen that the pressure does not depend on y , and hence u_x can be found from equation (3.8a), by using no-slip boundary conditions at $y = 0$ and $y = h(x)$, as

$$u_x(x, y) = \frac{1}{2\eta} \frac{\partial p}{\partial x} (y^2 - yh(x)). \quad (3.9)$$

The gap $h(x)$ between the sphere and the channel walls is locally approximated by a parabola

$$h(x) = h_0 \left[1 + \frac{x^2}{2h_0 a} + \mathcal{O} \left(\frac{x^4}{h_0 a^3} \right) \right]. \quad (3.10)$$

The total flow rate, Q , is found by integrating the flow field (Eq. (3.9)) in the gap around sphere:

$$Q = 2\pi a \cos(\gamma) \int_0^{h(x)} u_x(x, y) dy = -\frac{\partial p}{\partial x} \frac{\pi a \cos(\gamma) h^3(x)}{6\eta}, \quad (3.11)$$

where the factor $2\pi a \cos(\gamma)$ comes from integrating along the circular gap of radius $a \cos(\gamma)$. Since the flow rate must be independent of x , the pressure drop across the sphere is

$$\Delta p = \int_{-\infty}^{\infty} \frac{\partial p}{\partial x} dx = \frac{6\eta Q}{\pi a \cos(\gamma)} \int_{-\infty}^{\infty} \frac{1}{h^3(x)} dx \quad (3.12a)$$

$$= \frac{9\eta Q}{2\sqrt{2} \cos(\gamma) (ah_0^5)^{1/2}} \quad (3.12b)$$

$$= \frac{9\eta Q}{2\sqrt{2} a^3 \cos \gamma (\beta \sin \gamma)^{5/2}}, \quad (3.12c)$$

where we have used that the gap size can be written as $h_0 = \beta a \sin(\gamma)$ in the final step. Note that the hydraulic resistance $R = \Delta p/Q$ scales with the gap viscosity, thickness and sphere radius as $R \sim \eta a^{-1/2} h_0^{-5/2}$.

3.2. Force balance

To derive the flow-rate/pressure drop relation for the system, we proceed to determine the equilibrium position $z_{d,\text{eq}}$ of the sphere from the force balance Eq. (3.2), see Fig. 1(a). This leads to an expression for the equilibrium relative displacement $\beta_{\text{eq}} = z_{\text{eq}}/a$ which then used in Eq. (3.12c) to determine the resistance.

To model the extension spring we assume a linear spring force of

$$F_{\text{spring}} = -k\Delta z, \quad (3.13)$$

where k is the spring constant and Δz is the vertical displacement from the equilibrium position. Let z_0 be the equilibrium length when no pressure is applied and let z_{max} be the maximum extension of the spring, obtained when the sphere touches the inclined wall. For a sphere located a distance $z_d = \beta a$ above the contact point, the spring extension is $\Delta z = z_{\text{max}} - z_0 - \beta a$ and hence the spring force is given by $F_{\text{spring}} = -k(z_{\text{max}} - z_0 - \beta a)$.

The hydrodynamic force on the sphere is given by

$$F_{\text{hyd},i} = \int_{\partial\Omega} [-p\delta_{ij} + \eta(\partial_i u_j + \partial_j u_i)] n_j da \quad (3.14)$$

where we use the index notation and $\partial\Omega$ denotes the surface of the sphere. In the lubrication limit, we expect that the pressure-term dominates the vertical force on the sphere. The main pressure gradient occurs in a narrow region near the gap, and the pressure-force can thus be approximated by assuming constant pressures above ($p_0 + \Delta p$) and below (p_0) the sphere:

$$\begin{aligned} F_{\text{hyd}}^{(p)} &\simeq 2\pi a^2 (p_0 + \Delta p) \int_0^{\pi/2+\gamma} \cos(\theta) \sin(\theta) d\theta + 2\pi a^2 p_0 \int_{\pi/2+\gamma}^{\pi} \cos(\theta) \sin(\theta) d\theta \\ &= \pi a^2 \cos(\gamma)^2 \Delta p \end{aligned} \quad (3.15)$$

where θ is the angle measured from the vertical. To obtain the viscous force, we note

that in the lubrication approximation $\partial/\partial x \ll \partial/\partial y$, so the dominant term is

$$F_{\text{hyd}}^{(\text{visc})} \simeq 2\pi a \cos(\gamma) \eta \int_{-\infty}^{\infty} \frac{\partial u_x}{\partial y} \Big|_{y=h(x)} \cos(\gamma) dx = \frac{4\pi}{3} \cos^2(\gamma) \sin(\gamma) \beta a^2 \Delta p \quad (3.16)$$

where the prefactor $2\pi a \cos \gamma$ comes from integration around the contact line, and the factor $\cos \gamma$ in the integral from the force projection along the z -axis. Comparing the magnitude of the pressure (Eq. (3.15)) and viscous (Eq. (3.16)) forces, we find

$$\frac{F_{\text{hyd}}^{(\text{visc})}}{F_{\text{hyd}}^{(\text{p})}} = \frac{4}{3} \frac{h_0}{a}. \quad (3.17)$$

In our case, where $h_0 \ll a$, the pressure force is seen to dominate the hydrodynamic force on the sphere.

To find the vertical equilibrium position of the sphere, we now combine the spring force (3.13) and the pressure force (3.15) using the force-balance equation Eq. (3.2), and find

$$\pi a^2 \cos(\gamma)^2 \Delta p - k(z_d - a\beta) = 0 \quad (3.18)$$

where we have written the initial height as $z_d = z_0 - z_{\text{max}}$. This leads to an expression for the relative position β at equilibrium:

$$\beta = \frac{kz_d - \Delta p \pi a^2 \cos(\gamma)^2}{ka}. \quad (3.19)$$

Combining Eqns. (3.19) and (3.12c) leads to a non-linear pressure-dependent flow rate Q

$$Q = \frac{2\sqrt{2} \cos^6(\gamma) a^3}{9 \eta} \left(\frac{a\pi \sin(\gamma)}{k} \right)^{5/2} \left(\frac{kz_d}{\pi a^2 \cos^2(\gamma)} - \Delta p \right)^{5/2} \Delta p. \quad (3.20)$$

Introducing the low-pressure-limit resistance

$$R_0 = \frac{9}{2\sqrt{2} \sin(\gamma)^{5/2} \cos(\gamma)} \frac{\eta}{(az_d^5)^{1/2}} \quad (3.21)$$

and the critical pressure drop Δp_c that makes the ball block the channel

$$\Delta p_c = \frac{kz_d}{\pi a^2 \cos^2(\gamma)}, \quad (3.22)$$

leads to a convenient expression for the flow rate:

$$Q = \frac{\Delta p}{R_0} (1 - \Delta p / \Delta p_c)^{5/2}. \quad (3.23)$$

When $\Delta p \ll \Delta p_c$ the flow rate scales linearly with pressure drop Δp , in accord with experimental observations (Fig. 2). A maximum in the flow rate occurs at the pressure drop $\Delta p_{\text{max}} = \frac{2}{7} \Delta p_c$, above which the valve gradually closes and the flow rate Q starts to decay.

3.3. Comparison between experiment and theory

The lubrication-theory model for the flow rate Q (Eq. (3.20)) captures the essential qualitative behavior of the experiment data (Fig. 2), and we find good quantitative agreement between experiments and theory with no free parameters. Moreover, the data collapsed onto a single line when scaled according to the maximum flow rate Q_{max} and corresponding pressure Δp_{max} (Fig. 3). The data collapse is seen to be in good accord

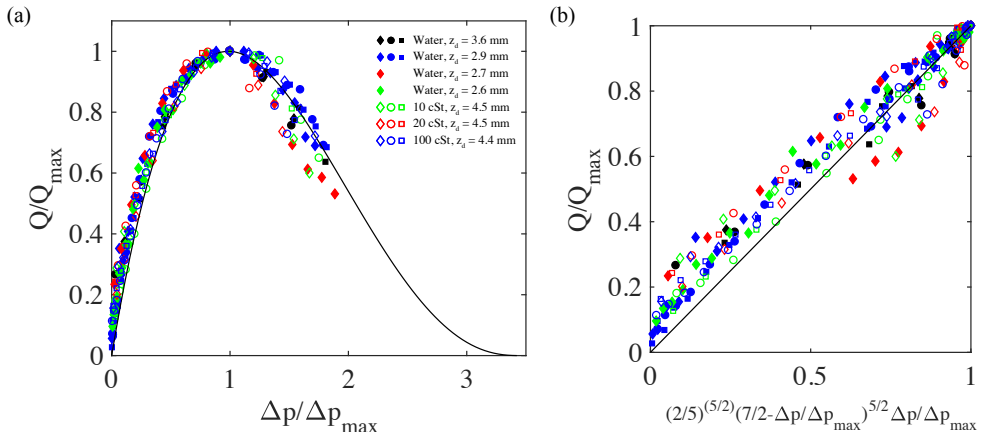


FIGURE 3. Normalized flow rate Q/Q_{\max} plotted as a function of (a) relative pressure drop $\Delta p/\Delta p_{\max}$ and (b) $(\frac{2}{5})^{5/2} \left(\frac{7}{2} - \frac{\Delta p}{\Delta p_{\max}}\right)^{5/2} \frac{\Delta p}{\Delta p_{\max}}$, using data from Fig. 2 (a,b). The solid line shows the theoretical prediction obtained using lubrication theory (Eq. (3.24)).

with the prediction from Eq. (3.23), which yields

$$\frac{Q}{Q_{\max}} = \left(\frac{\Delta p_c - \Delta p}{\Delta p_c - \Delta p_{\max}}\right)^{5/2} \frac{\Delta p}{\Delta p_{\max}} = \left(\frac{2}{5}\right)^{5/2} \left(\frac{7}{2} - \frac{\Delta p}{\Delta p_{\max}}\right)^{5/2} \frac{\Delta p}{\Delta p_{\max}}, \quad (3.24)$$

where we have used that the maximum pressure is $\Delta p_{\max} = 2/7\Delta p_c$.

4. Discussion and conclusion

In this paper we have presented an experimental and theoretical study of a bioinspired soft valve. The model system comprised a sphere connected to a spring located inside a tapering channel. A coupling between elasticity and fluid motion determines the hydraulic resistance of the valve because the position of the sphere is influenced by the flow and vice versa. Using a simple setup, we performed experiments to characterize the pressure-drop/flow rate relationship for the system. Our data revealed a strongly non-linear behaviour and the existence of an optimal pressure drop for the system where the flow rate is maximized.

Assuming low-Reynolds-number flow, we proposed a mathematical model that reduced the complexity of the flow to a two-dimensional lubrication approximation. The model revealed a relatively complete picture of the geometric and material parameters that affect flow through the system. The model predictions compared favorably to the results of our experiments. Our analysis is limited to steady viscous flows, though preliminary observations suggest onset of self-excited oscillations at higher Reynolds numbers.

Acknowledgements

This work was supported by a research grant (13166) from VILLUM FONDEN.

REFERENCES

- BELLHOUSE, B. J. & TALBOT, L. 1969 The fluid mechanics of the aortic valve. *Journal of Fluid Mechanics* **35** (4), 721–735.

- CHAPMAN, DC, RAND, RH & COOKS, JR 1977 A hydrodynamical model of bordered pits in conifer tracheids. *Journal of theoretical biology* **67** (1), 11–24.
- CHOAT, BRENDAN, COBB, ALEXANDER R & JANSEN, STEVEN 2008 Structure and function of bordered pits: new discoveries and impacts on whole-plant hydraulic function. *New phytologist* **177** (3), 608–626.
- DUPRAT, CAMILLE & STONE, HOWARD A 2015 *Fluid-Structure Interactions in Low-Reynolds-Number Flows*. Royal Society of Chemistry.
- GART, SEAN, SOCHA, JOHN J, VLACHOS, PAVLOS P & JUNG, SUNGHWAN 2015 Dogs lap using acceleration-driven open pumping. *Proceedings of the National Academy of Sciences* **112** (52), 15798–15802.
- GROTBERG, JAMES B & JENSEN, OLIVER E 2004 Biofluid mechanics in flexible tubes. *Annu. Rev. Fluid Mech.* **36**, 121–147.
- HEIL, MATTHIAS & HAZEL, ANDREW L 2011 Fluid-structure interaction in internal physiological flows. *Annual review of fluid mechanics* **43**, 141–162.
- HEIL, MATTHIAS & HAZEL, ANDREW L 2015 Flow in flexible/collapsible tubes. In *Fluid-Structure Interactions in Low-Reynolds-Number Flows* (ed. Camille Duprat & Howard Stone), pp. 280–312. Royal Society of Chemistry.
- HOLMES, DOUGLAS P, TAVAKOL, BEHROUZ, FROEHLICHER, GUILLAUME & STONE, HOWARD A 2013 Control and manipulation of microfluidic flow via elastic deformations. *Soft Matter* **9** (29), 7049–7053.
- JENSEN, KAARE H, BERG-SØRENSEN, KIRSTINE, BRUUS, HENRIK, HOLBROOK, N MICHELE, LIESCHE, JOHANNES, SCHULZ, ALEXANDER, ZWIENIECKI, MACIEJ A & BOHR, TOMAS 2016 Sap flow and sugar transport in plants. *Reviews of modern physics* **88** (3), 035007.
- KIM, WONJUNG & BUSH, JOHN WM 2012 Natural drinking strategies. *Journal of Fluid Mechanics* **705**, 7–25.
- LANCASHIRE, JR & ENNOS, AR 2002 Modelling the hydrodynamic resistance of bordered pits. *Journal of Experimental Botany* **53** (373), 1485–1493.
- LEDESMA-ALONSO, R, GUZMÁN, JEV & ZENIT, R 2014 Experimental study of a model valve with flexible leaflets in a pulsatile flow. *Journal of Fluid Mechanics* **739**, 338–362.
- LUO, XY & PEDLEY, TJ 1996 A numerical simulation of unsteady flow in a two-dimensional collapsible channel. *Journal of Fluid Mechanics* **314**, 191–225.
- MCCULLOH, KATHERINE A, SPERRY, JOHN S & ADLER, FREDERICK R 2003 Water transport in plants obeys murray’s law. *Nature* **421** (6926), 939.
- PARK, KEUNHWAN, KIM, WONJUNG & KIM, HO-YOUNG 2014 Optimal lamellar arrangement in fish gills. *Proceedings of the National Academy of Sciences* **111** (22), 8067–8070.
- SCHULTE, PAUL J 2012 Computational fluid dynamics models of conifer bordered pits show how pit structure affects flow. *New Phytologist* **193** (3), 721–729.
- SMISTRUP, KRISTIAN & STONE, HOWARD A 2007 A magnetically actuated ball valve applicable for small-scale fluid flows. *Physics of Fluids* **19** (6), 063101.
- SOTIROPOULOS, FOTIS, LE, TRUNG BAO & GILMANOV, ANVAR 2016 Fluid mechanics of heart valves and their replacements. *Annual Review of Fluid Mechanics* **48**, 259–283.
- WEXLER, JASON S, TRINH, PHILIPPE H, BERTHET, HELENE, QUENNOUZ, NAWAL, DU ROURE, OLIVIA, HUPPERT, HERBERT E, LINDNER, ANKE & STONE, HOWARD A 2013 Bending of elastic fibres in viscous flows: the influence of confinement. *Journal of fluid mechanics* **720**, 517–544.
- YANG, PATRICIA J, PHAM, JONATHAN, CHOO, JEROME & HU, DAVID L 2014 Duration of urination does not change with body size. *Proceedings of the National Academy of Sciences* **111** (33), 11932–11937.

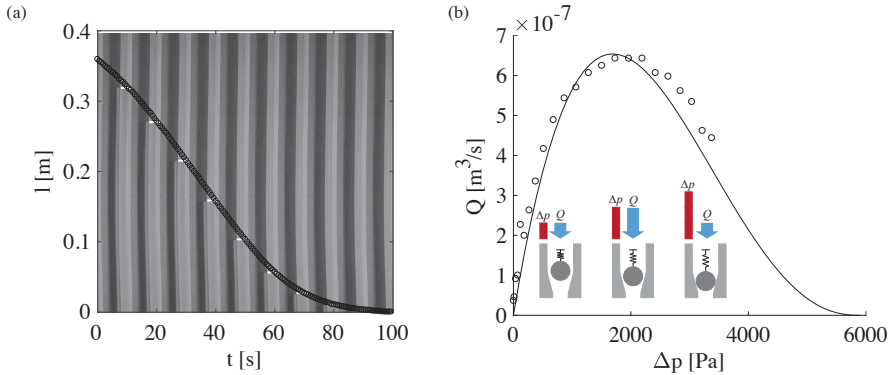


FIGURE 4. Experimental result of $z_d = 2.9$ mm with water. (a) Time vs liquid column height graph with a montage of every 10s images. Tracking points (Circles) is well fitted with experimental images (Horizontal white lines). (b) Pressure drop and flow rate graph from (a). inset shows the ball position at certain pressure drop.

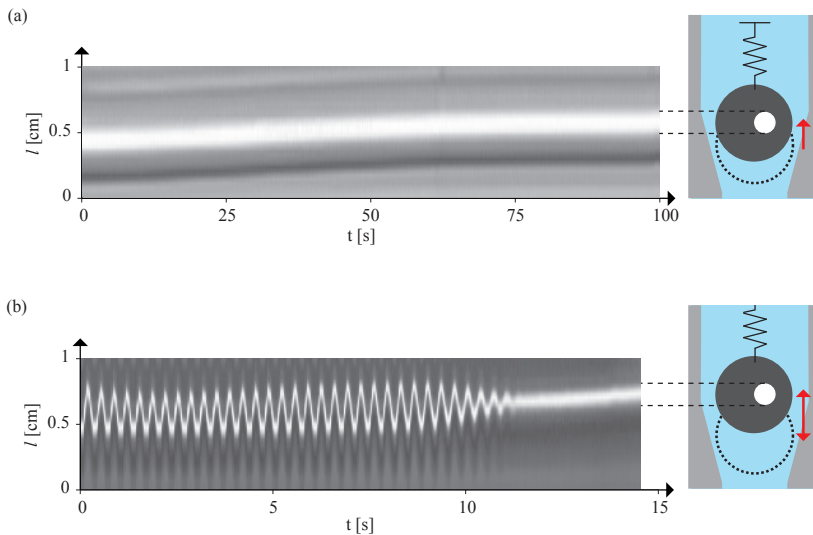


FIGURE 5. (a) Experimental kymograph of a soft valve with water and $z_d = 2.9$ mm. Image variation shows ball movement during the experiment (see Supplemental movie1). (b) Kymograph of a soft valve with water and $z_d = 5.4$ mm. During the first 10 seconds the valve oscillates and then moves softly. Pressure drop decreases from 7500 Pa. The oscillation stops when the Reynolds number between the gap is less than 2700 (see Supplemental movie2).

Appendix A. Tracing the meniscus

The pressure-drop/flow rate relation was determined experimentally as outline in Fig.1(c) and Fig. 4. A stack of images showing the meniscus movement was converted to gray-scale and cropped to show the silicone tube above the soft valve. The 2D-images $I(z, x, t)$ were converted to a 1D intensity profile $I'(z, t) = \sum_x I(z, x, t)$ by summing the values in each horizontal image row. We traced the position of the meniscus by locating the maximum in the intensity gradient $\sim \partial_z I'(z, t)$ at the position $z_{\max}(t)$. This yielded the meniscus position $z_{\max} = l(t)$ which in turn allowed us to determine the flow rate Q . In order to minimize effects of image noise in determining z_{\max} , we manually indicated the initial meniscus position and used a tracing window.